International Journal of Heat and Mass Transfer 52 (2009) 1794–1801

Contents lists available at ScienceDirect

International Journal of Heat and Mass Transfer

journal homepage: www.elsevier.com/locate/ijhmt

Numerical study of the relationship between heat transfer enhancement and absolute vorticity flux along main flow direction in a channel formed by a flat tube bank fin with vortex generators

Li-Min Chang, Liang-Bi Wang *, Ke-Wei Song, Dong-Liang Sun, Ju-Fang Fan

Department of Mechanical Engineering, Lanzhou Jiaotong University, Lanzhou, Gansu 730070, PR China

ARTICLE INFO

Article history:
Received 10 March 2008
Received in revised form 11 August 2008
Available online 4 December 2008

Keywords:
Vortex generator
Convective heat transfer
The secondary flow
Vorticity flux
Absolute vorticity flux

ABSTRACT

The secondary flow is frequently used to enhance the convective heat transfer. In this paper, the cross-averaged absolute vorticity flux in the main flow direction is used to specify the intensity of the secondary flow produced by vortex generators that are mounted on a three-row flat tube bank fin surfaces. The relationship between the intensity of the secondary flow and the strength of convective heat transfer is studied using a numerical method. The results reveal that cross-averaged absolute vorticity flux in the main flow direction can reflect the intensity of the secondary flow; a significant relationship between this cross-averaged absolute vorticity flux and span-averaged Nusselt number exists for the case studied. This cross-averaged absolute vorticity flux can account only for the secondary flow effects on convective heat transfer but cannot quantify the effects of developing boundary layer on convective heat transfer.

1. Introduction

In tube bank fin heat exchangers, the airside resistance generally comprises more than 90% of the total thermal resistance. Therefore, special surfaces are employed to effectively improve the airside heat transfer performance of tube bank fin heat exchangers. Vortex generators (VGs) can be applied on the fin surface to generate longitudinal vortices in the main flow; hence, the heat transfer of the fin surface is enhanced. There are many reported results of the studies in this branch [1–20]. These results mainly report the effects of the geometrical configurations of VGs, such as the positions VGs are located, the attack angle of VGs, the arrangement of VGs, and the shape of VGs on heat transfer and pressure loss. The methods used in these studies are experimental and numerical. A large number of useful insights on the mechanism of the heat transfer enhancement using VGs have been obtained. The most recently results [21] show that the vortices generated by different VGs will interact with each other, and such interactions will have influences on heat transfer enhancement.

Although there are the terms *common flow down* and *common flow up* to distinguish the role of vortex generator pair [13], the key point of heat transfer enhancement using VGs is the secondary flow produced by the VGs. It is not clear why the secondary flow will have efficient enhancement on convective heat transfer even if such flow is weaker than the main flow. The answer may be found from field synergy [22]. But one faces a fundamental challenge: Except in some special cases, there is no parameter that can be used to specify the intensity of the secondary flow.

If the heat transfer enhancement method using the secondary flow is considered, there are other methods. Tubes with helical ribs have been used as one of the passive heat transfer enhancement techniques; they are the most widely used tubes in several heat transfer applications such as heat recovery processes, air conditioning and refrigeration systems, and chemical reactors [23–25].

The use of a twisted-tape insert is an effective method to improve the convective heat transfer of laminar flow in the tube, since it offers significant increase in heat transfer as compared with the pressure drop, particularly at high Prandtl numbers [26–31].

In above-mentioned methods using the secondary flow to enhance convective heat transfer, except for the twisted-tape inserts, few published papers have reported a parameter that can specify the intensity of the secondary flow. For the tube with the twisted-tape insert case, there is a parameter called *swirl parameter*, but it cannot be used in more general cases. Like twisted-tape inserts, it is expected that for the secondary flow, there should exist a parameter that can specify its strength with more general consideration than in the case of the twisted-tape insert. The other work should be to connect this parameter with the intensity of heat transfer. For real applications, this parameter should be used to revaluate the goodness of the arrangement of secondary flow producers such as VGs on fin surface. In this paper, we show such parameter and find the relationship between this parameter and

* Corresponding author. Tel./fax: +86 931 4956556.
E-mail address: lbwang@mail.lzjtu.cn (L.B. Wang).

0017-9310/$ - see front matter © 2009 Published by Elsevier Ltd.
doi:10.1016/j.ijheatmasstransfer.2008.09.029

Nomenclature

A	cross-section area of flow passage [m^2]
a	width of flat tube [m]
b	length of flat tube [m]
d_h	characteristic length [m]
f	friction factor: $f = \Delta p d_h/(L\rho u_m^2/2)$
h	heat transfer coefficient [$W/m^2 s$]
H	height of winglet type vortex generators [m]
J^n	vorticity flux in normal direction of cross-section [s^{-1}]
J^n_{ABS}	cross-averaged absolute vorticity flux in normal direction [s^{-1}]
$J^n_{ABS,S}$	stream wise averaged J^n_{ABS}[s^{-1}]
L	stream wise length of fin [m]
n	direction normal to the cross-section or wall surface [m]
Nu	Nusselt number: $Nu = hd_h/\lambda$
Re	Reynolds number: $Re = \rho \cdot u_{max} \cdot d_h / \mu$
S_1	transversal pitch of flat tubes [m]
S_2	longitudinal pitch of flat tubes [m]
T_p	fin spacing [m]
T	temperature [K]
u_m	maximum velocity [m/s]
u	average velocity of air [m/s]
u_i, u, v, w	u, v, w components of velocity vector [m/s]

Greeks

η	coordinate
λ	heat conductivity [W/m K]
μ	viscosity [$kg/m^2 s$]
ρ	density [kg/m^3]
θ	attack angle of vortex generator [°]
Θ	dimensionless temperature [−]
Δ	small interval
Δp	pressure drop [Pa]
ω	vorticity [s^{-1}]
Γ	circulation of velocity [$m^2 s^{-1}$]
ξ, ζ	coordinator axes

Subscript

bulk	cross-averaged value
local	local value
m	averaged value
w	wall or fin surface

the enhancement of heat transfer in the case of flat tube bank fin mounted with VGs.

2. Problem studied and its mathematic formulation

A flat tube bank fin with three-row tubes as shown in Fig. 1 is studied. The arrangement of the tube and the positions of VGs are shown in Fig. 2(a). The geometry of the fin pattern of the tube bank fin heat exchanger is based on a typical locomotive radiator. To validate the suitability of the numerical method used in this paper, we selected the geometry of the fin pattern used in naphthalene sublimation experiments, where the geometry of locomotive radiator is enlarged with a factor of 2.5. If this factor is considered, the fin spacing is in the normal region: 1.6–2.4 mm.

The geometry of VG is shown in Fig. 2(b). The tube length b is 46.3 mm; the tube width a is 6.3 mm; the transversal pitch between flat tubes S_1 is 40 mm; the longitudinal pitch between flat tubes S_2 is 55 mm; the span distance between two VGs δ is 12.6 mm; the angle of attack θ is 35°; the base length and height of the VG are 8.0 and 4.0 mm, respectively; three types of fin spacing, T_p = 4.0, 5.0, and 6.0 mm, are selected.

The flow and heat transfer are assumed to be incompressible and in a steady state. The studied domain is selected as shown in Fig. 3. The physics of the problem studied can be described by the compact forms of governing equations:

Continuity equation

$$\frac{\partial}{\partial x_i}(\rho u_i) = 0 \tag{1}$$

Momentum equation

$$\frac{\partial}{\partial x_i}(\rho u_i u_k) = \frac{\partial}{\partial x_i}\left(\mu \frac{\partial u_k}{\partial x_i}\right) - \frac{\partial p}{\partial x_k} \quad (k = 1,2,3) \tag{2}$$

Energy equation

$$\frac{\partial}{\partial x_i}(\rho c_p u_i T) = \frac{\partial}{\partial x_i}\left(\lambda \frac{\partial T}{\partial x_i}\right) \tag{3}$$

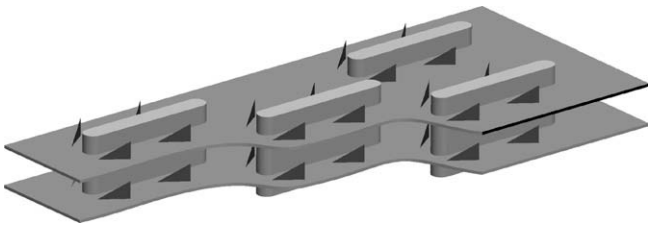

Fig. 1. Schematic view of a finned three-row flat tube bank with mounted VGs.

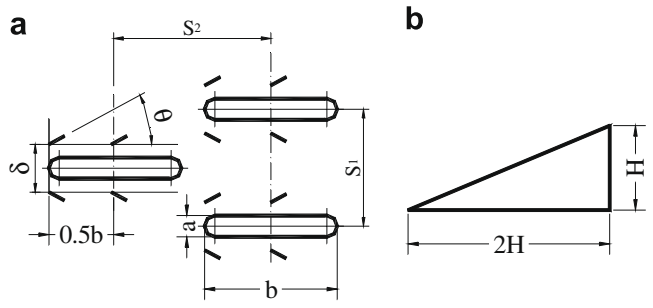

Fig. 2. Flat tube bank parameters and positions where VGs were mounted, (a) configuration and (b) shape of VG.

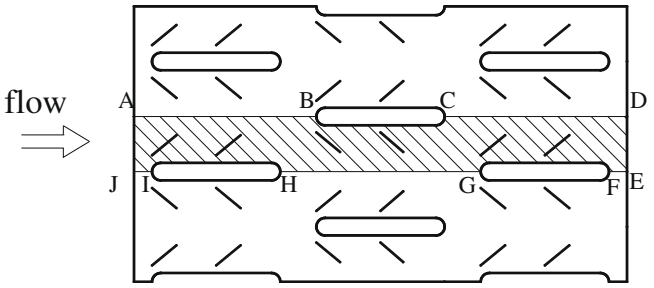

Fig. 3. Simulation domain and indication of boundary.

The boundary conditions are

at inlet cross-section of fluid flow (AJ in Fig. 3):

$$u(x,y,z)=u_{\text{in}},v(x,y,z)=0,w(x,y,z)=0,T(x,y,z)=T_{\text{in}} \tag{4}$$

at outlet cross-section of fluid flow (DE in Fig. 3):

$$\frac{\partial}{\partial x}u(x,y,z)=0,\frac{\partial}{\partial x}v(x,y,z)=0,\frac{\partial}{\partial x}w(x,y,z)=0,\frac{\partial}{\partial x}T(x,y,z)=0 \tag{5}$$

on symmetric surfaces(AB, CD, JI, HG, FE in Fig. 3):

$$v(x,y,z)=0,\frac{\partial}{\partial n}u(x,y,z)=0,\frac{\partial}{\partial n}w(x,y,z)=0,\frac{\partial}{\partial n}T(x,y,z)=0 \tag{6}$$

on the fin surfaces:

$$u(x,y,z)=0,v(x,y,z)=0,w(x,y,z)=0,T=T_w \tag{7}$$

The Reynolds number and the friction factor are defined as:

$$Re=\rho\cdot u_{\text{m}}\cdot d_{\text{h}}/\mu \tag{8}$$

$$f=\Delta p d_{\text{h}}/(L\rho u_{\text{m}}^2/2) \tag{9}$$

The Reynolds number is selected from the working condition of a typical locomotive radiator. This type of radiator has a working velocity of about 10 m/s of air and a flat tube with a width of 2.5 mm; in this condition, the Re_{a} is about 1300 (using the characteristic length of flat tube width, 2.5 mm).

To compare the numerical results with the experimental results, in this paper we used the width of the tube as characteristic length, $d_{\text{h}}=a$.

The local heat transfer coefficient is determined by the following equation

$$H_{\text{local}}=\left(-\lambda\frac{\partial T}{\partial n}\right)\Big/(T_{\text{w}}-T_{\text{bulk}}) \tag{10}$$

Local heat transfer coefficient is averaged over total surface involved in heat transfer (except the surface of VGs) to obtain the averaged h_{m}. The local and average Nusselt number are determined by

$$Nu_{\text{local}}=h_{\text{local}}\cdot d_{\text{h}}/\lambda \quad\text{and}\quad Nu_{\text{m}}=h_{\text{m}}\cdot d_h/\lambda \tag{11}$$

As mentioned above, the focus of this paper is to find a parameter to specify the intensity of the secondary flow. Before further process can be made, the next step is to select this parameter.

3. Selecting the parameter to quantify the intensity of the secondary flow

Generally speaking, the secondary flow is a flow on cross-section normal to main flow. This flow does not need to be a swirling movement of fluid. In most cases, the swirl of fluid is described by the word of "vortex". Here we referred to Treffethen and Panton's statement: "There seems to be no good working definition of vortex, in spite of the fact that vorticity is well defined mathematically $\boldsymbol{\omega}=\nabla\times\boldsymbol{v}$. The term may have to remain as a vague category for various swirling motions" [32]. Fiebig added this statement with that combined expressions such as vortex line, vortex street, vortex element, and numerous others are well defined [1]. According to Fiebig's description, the vortex should be that the flow moves around a common center, with

$$\boldsymbol{\omega}=\nabla\times\boldsymbol{v}\neq 0 \tag{12}$$

$$\Gamma=\oint_L \boldsymbol{v}\cdot d\boldsymbol{l}=\int\int_w \boldsymbol{\omega}\cdot d\boldsymbol{A}\neq 0 \tag{13}$$

The other requirement is flow has re-circulation.

For the secondary flow, it really meets the requirement as indicated in Eq. (12), but does not always meets the requirements of re-circulation and Eq. (13). There is no clear definition about the vortex as mentioned above, inferring from the definition of vorticity, here we use a statement that the secondary flow is the combination of vortices. In this case, the secondary flow can be quantified by vorticity with some special treatments. Vorticity has three components respecting to commonly used x, y and z coordinates. If the secondary flow is considered, we use the component normal to the cross-section to describe the intensity of the secondary flow. This direction is aligned with the direction of heat transfer in fluid flow because moving fluid transports heat along the main flow direction.

$$J^n=\int\int_A \omega^n dA \tag{14}$$

It is found that this vorticity flux can describe only the intensity of the secondary flow when just one vortex exists in the cross-section and the secondary flow on the cross-section without a solid boundary. If more than one vortex exists in cross-section, especially with counter-rotating direction, J^{n} will be reduced or counter-balanced [21]. If the cross-section has a solid boundary, J^{n} is zero. In such cases, although every vortex will contribute to the convection, J^{n} specifies only the overall results of vorticity flux. In order to overcome this shortcoming of using Eq. (14) as the description of the intensity of the secondary flow, we use following definition

$$J^n_{\text{ABS}}=\frac{\int\int_A \mid\omega^n\mid dA}{A} \tag{15}$$

The absolute vorticity flux J^n_{ABS} denotes the averaged absolute vorticity flux of all of vortices over the unit area of cross-section, it includes all vortices on this cross-section, and so it is expected to describe the intensity of the secondary flow.

In order to get the absolute vorticity flux, velocity field information is necessary. There is no experiment can get detailed information of velocity field, a numerical method is used here.

4. Numerical method and its validation

The numerical method used is the finite volume method with structure grid system. The power scheme is used to discretize the convective terms. SIMPLE algorithm [33] is used to handle the coupling between velocity and pressure. The collocation grid arrangement is used to easily treat of VGs penetrating into the flow. To ensure the coupling between velocity and pressure, the momentum interpolation of Rhie and Chow [34] is adopted to determine the interface velocity. VGs mounted on the surface are simulated by a solid slice immersed in the flow as indicated in Fig. 4(c). The numerical method of treating the solid slice immersed in the flow is reported in Ref. [35].

To handle the complex of simulated domain, the governing equations shown above are then transformed into governing equations in the computational space. The simulation domain in the physical space (x–y–z coordinates) is also transformed into a rectangular parallelepiped in the computational space (ξ–η–ζ coordinates) by using the multi-surface algebraic method [36]. The schematic view of the grid system in physical space is shown in Fig. 4.

It is possible to have a smooth interpolation of the grid points and create the winglets of zero thickness [37,38]; however, this method also has shortcomings such as the real thickness of vortex generator is not zero, and for the winglet VGs, this method is also stepwise in the direction along the height of VGs. The

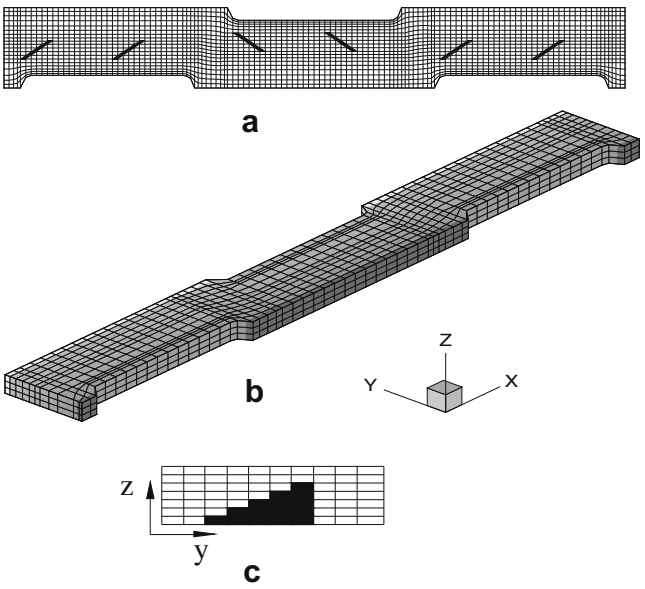

Fig. 4. Schematic view of grid system used in simulation, (a) locations of VGs and grid in plane of x–y, (b) grid system, (c) projective view of the treatment of VGs.

boundary-conforming treatment of the winglet VGs can be realized only with the unstructured grid system.

The non-boundary-conforming grid about the vortex generators may not be able to capture the full physics of the winglet vortex or introduce inaccuracy in some degree. But after carefully checking, it is found that the step wing treatment of VGs can produce good agreement between local Nusselt numbers obtained by numerical and experimental methods. The comparison of the local results of Nusselt numbers is presented elsewhere. It is sure that step wing treatment of VGs will bring the inaccuracy of local flow field; however, the size of VGs is small compared to the length in which vortices produced by VGs can penetrate along the main flow direction, such inaccuracy of local flow field is acceptable if finer grid system is used in simulation.

In present simulation computations are conducted for three cases, T_p = 4, 5, and 6 mm, at certain Reynolds numbers. Grid independence study are performed at Re = 1136, 1121, and 1076, respecting to the experiments. Three grid sizes are used for each case, shown in Table 1. The difference in the average Nusselt number and friction factor between three results for each case are both less than 3%, and the solutions presented in this paper is obtained using the grid of 345 × 44 × 13, 345 × 44 × 16, 345 × 44 × 19 for each fin spacing, respectively.

Before further simulation is carried out, fluid flow and heat transfer in the configuration, adopted in the experimental study, was simulated in order to validate the suitability of numerical method. The numerical results of averaged Nu and f are compared with the experimental data reported in Ref. [8]. The detail of the experiment will not be repeated here, but it should be emphasized that in numerical analyses, the same configuration and the same boundary conditions of experimental surfaces are used. For the naphthalene sublimation experiment, the exact boundary condition of surface sublimation that takes place is isotherm condition. In experimental study, an experimental model with a factor of 2.5 to real application size is used; hence, in real application, all geometry sizes should multiply by a factor of 1/2.5.

Table 1
Grid dependence of numerical results.

Re	T_p (mm)	Grid ($x \times y \times$ i)	Nu	f
1136	4	282 × 39 × 11	11.03	0.1564
	4	315 × 39 × 12	11.01	0.1587
	4	345 × 44 × 13	11.00	0.1612
1121	5	282 × 39 × 13	10.41	0.1210
	5	315 × 39 × 15	10.11	0.1176
	5	345 × 44 × 16	10.15	0.1194
1076	6	282 × 39 × 16	9.05	0.0926
	6	315 × 39 × 17	9.08	0.0939
	6	345 × 44 × 19	8.95	0.0912

For T_p = 4 mm, in region of Reynolds number studied, a good agreement between numerical and experimental results is obtained, with the relative error of Nu below 5%. For T_p = 5 mm, good agreement is obtained only when Re < 1200. The largest relative error of Nu occurs near Re = 1600, which has a value of 9.8%. For T_p = 4 mm, except small Re, a good agreement between numerical and experimental results of f is obtained. The largest relative error occurs near Re = 500, which has a value of 7.9%. With the increasing of Re, the relative error of f decreases. For T_p = 5 mm, a good agreement in f is obtained in Re region studied. The largest relative error occurs near Re = 400, which has a value of 5.2%.

For T_p = 4 mm, the local Nusselt number on the fin surfaces mounted with VGs (fin surface I) and without VGs (fin surface II) formed the same channel, as presented in Figs. 5 and 6, respectively. We will not explain these figures in details. These figures indicate that the numerical method used in this paper can reasonably reproduce most significant characteristics of the local Nusselt distributions obtained by experimental method both on fin surfaces I and II. The above-mentioned facts demonstrate the suitability of the numerical method used.

5. Results and discussion

The outline of presentation of results is: Firstly, we show that J^n_{ABS} can be used to describe the intensity of secondary flow; then, the relationship of J^n_{ABS} with Nusselt number is presented.

5.1. Relationship between J^n_{ABS} and the intensity of the secondary flow

Fig. 7 shows the distribution of J^n_{ABS} along stream wise. The absolute vorticity flux decreases with the increasing of T_p. Because in the inlet region, the secondary flow is not strong, in this region J^n_{ABS} has the minimum value. J^n_{ABS} increases with developing of flow. There are peak values both in front of the tube and in position where VGs located. Around the first tube, in position of the second VG located, is larger than that in position of the first VG located, and in the region behind the second VG, J^n_{ABS} is also larger than that behind the first VG. Around the second and the third tubes, in the position of the second VG the value of J^n_{ABS} is weaker than that in position of the first VG; this trend is contrary to the case around the first tube. The peak values located at leading edge of the second tube is larger than that at leading edge of the third tube. The peak values located around the second VG of the three tubes are nearly equal. As expected, it is found that J^n_{ABS} decreases along the stream direction after every VG.

Fig. 8 shows the velocity vectors on 16 cross-sections along stream wise for T_p = 5 mm, Re = 1121. These series of velocity vector fields clearly show the development of vortices in the channel formed by the flat tube bank fins. These fields also present the intensity of the secondary flow. The positions of these cross-sections are at x/S_2 = 0.053, 0.259, 0.378, 0.697, 0.817, 1.0190, 1.272, 1.392, 1.711, 1.830, 2.007, 2.259, 2.378, 2.711, 2.830, and 2.981. On the section near the inlet region before the changing of the channel area, the secondary flow is weak; this can be seen on cross-section at x/S_2 = 0.062 in Fig. 8(a), and from Fig. 7 it is found at this location J^n_{ABS} is small. On cross-section the leading edge of

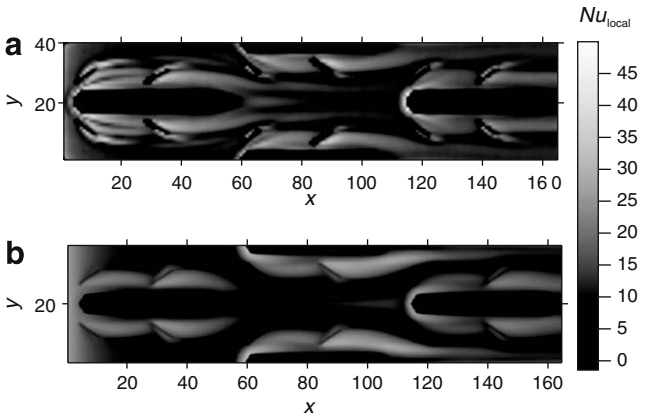

Fig. 5. Comparison of experimental and numerical simulation results of local *Nu* distribution on fin surface I for T_p = 4 mm and *Re* = 1136, (a) experimental results on fin surface I and (b) numerical results on fin surface I.

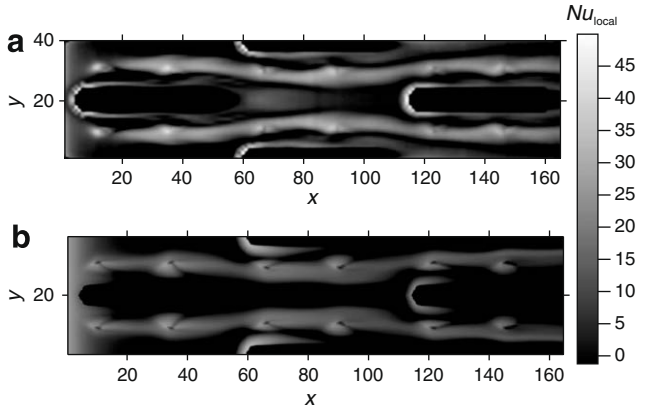

Fig. 6. Comparison of experimental and numerical simulation results of local *Nu* distribution on fin surface II for T_p = 4 mm and *Re* = 1136, (a) experimental results on fin surface II and (b) numerical results on fin surface II.

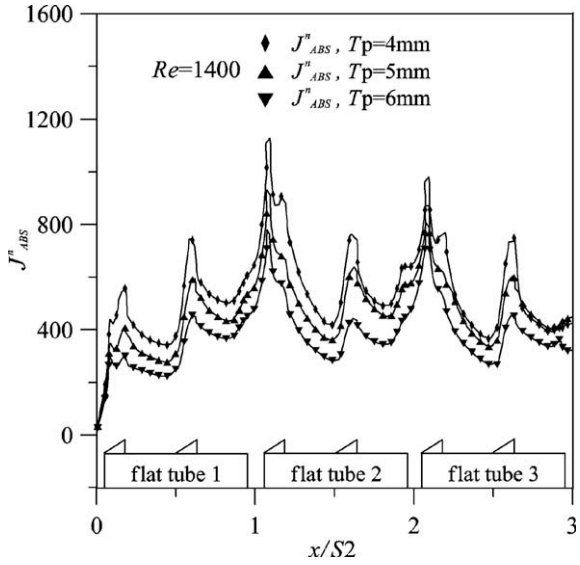

Fig. 7. Distribution of span-averaged J^n_{ABS}.

VGs located, Fig. 8(b), a strong secondary flow is generated, and at this location a peak value of J^n_{ABS} in Fig. 7 is found. The intensity of the secondary flow decreases behind the first VG, see Fig. 8(c). When the flow passes through the second VG, the secondary flow becomes strong again, see Fig. 8(d); farther downstream, the strength of the secondary flow becomes weak behind the second VG, see Fig. 8(e). Comparing Fig. 8(b) and (d), one finds that the secondary flow is stronger in the region around the second VG than around the first VG. Comparing Fig. 8(c) and (e), we can find that the secondary flow is also stronger behind the second VG than behind the first VG. On the section located between the first and the second tubes, shown in Fig. 8(f), it is found that the secondary flow

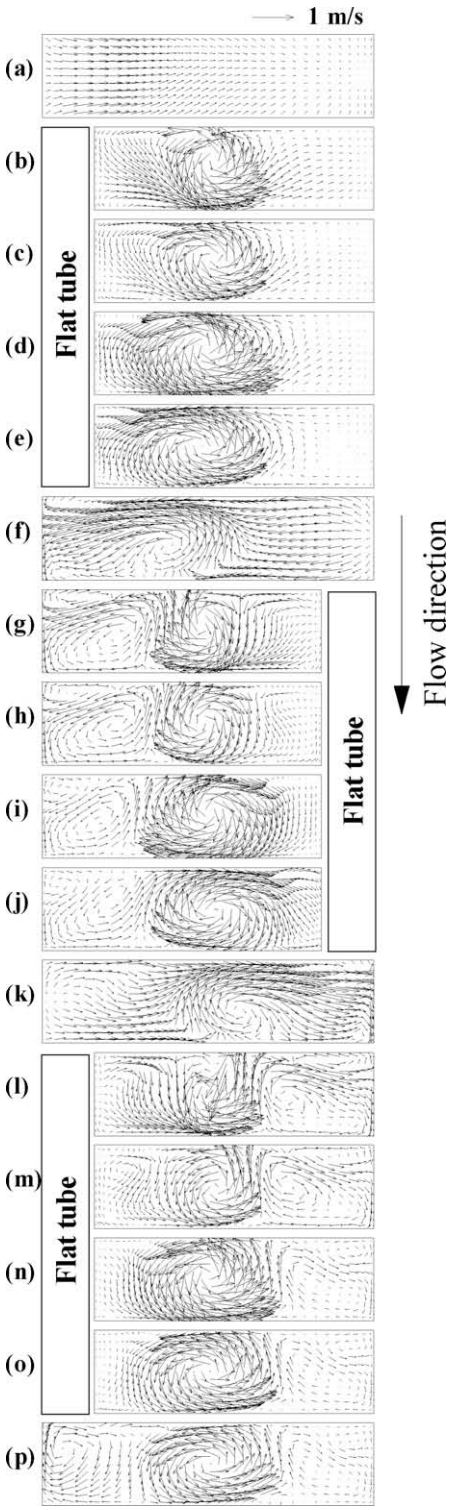

Fig. 8. Velocity field on different cross-sections.

generated by the VGs becomes weaker if Fig. 8(e) is used as reference. Around the second flat tube, see Fig. 8(g) to (j), there exist two main vortex systems on each cross-section; the vortex system far away from the second tube comes from the upstream, which is generated by VGs around the first row tube. Another vortex system is generated by the VGs around the second row tube. The secondary flow is stronger behind the second VG than behind the first VG; this trend is similar to the flow around the first tube. The secondary flow coming upstream decreases continually downstream; it becomes weak on the section located between the second and the third row tubes, shown in Fig. 8(k). Around the third row tube, shown in Fig. 8(l) to (o), the characteristic is similar to the case on cross-sections around the second row tube. Comparing the distribution of J^n_{ABS} with the development of velocity vector fields on different cross-sections along stream wise, we can find that J^n_{ABS} really reflects the intensity of the secondary flow.

It is found that on the cross-sections located in the second tube row, the vortices produced by the VGs around the first tube row are in counter-rotation direction with the vortices produced by the VGs around the second tube row. If we use only vorticity to describe the secondary flow intensity, the averaged vorticity intensity will be reduced. In such case, averaged vorticity cannot describe the intensity of the secondary flow; however, absolute vorticity intensity can reflect the intensity of the secondary flow formed by two or more vortex systems with different rotation direction.

Some evidences can also be found in Fig. 9. This figure shows the distributions of J^n_{ABS} on the same sections in Fig. 8. On the cross-section near the inlet region, the flow direction changed, strong secondary flow generated near the fin surfaces, there has largeonly in region close to the fin surfaces, this can be seen on cross-section at $x/S_2 = 0.053$ in Fig. 9(a). In the section behind the first VG, shown in Fig. 9(b), there has strong secondary flow generated by the first VG, there has large J^n_{ABS} both in the region behind the VG and the regions adjacent to the fin surfaces. J^n_{ABS} behind the first VG decreases downstream, shown in Fig. 9(c). When the flow passes the second VG, as shown in Fig. 9(d), the strength of J^n_{ABS} near the tube become stronger than that behind the VG, and the strength of J^n_{ABS} in this section is large compared with J^n_{ABS} in the section behind the first VG shown in Fig. 9(b). The strength of J^n_{ABS} decreases downstream the second VG, as shown in Fig. 9(e). Fig. 9(f) shows J^n_{ABS} on the section located between the first and second tubes, in this cross-section the value of J^n_{ABS} in flow core decreases greatly, but there has large J^n_{ABS} near top fin surface. On the cross-sections around the second tube row, see Fig. 9(g) to (j), the development of J^n_{ABS} caused by the VGs located in this region is similar as that on the cross-sections around the first row tube; the difference is that on these cross-sections, there are zones with high values of J^n_{ABS} behind the first row tube, and these zones locate far from the second row tube. The value of J^n_{ABS} in these zones decreases downstream until they meet the third row tube. On the cross-sections around the third row tube, see Fig. 9(l)–(o), it is found that the development of J^n_{ABS} is similar to the cases around the second row tube. Comparing the distributions of J^n_{ABS} on different cross-sections along stream wise with the development of velocity vector field on the corresponding cross-sections, it is found that that J^n_{ABS} can be used to quantify the intensity of the secondary flow.

The question we face now is that although J^n_{ABS} can be used to quantify the intensity of the secondary flow, what is the relationship between Nu_s and J^n_{ABS}?

5.2. Relationship between Nu_s and J^n_{ABS}

Distributions of span-averaged Nu_s and J^n_{ABS} at different fin spacing are shown in Fig. 10. The first conclusion can be made is that both Nu_s and J^n_{ABS} are affected by the fin spacing, because when

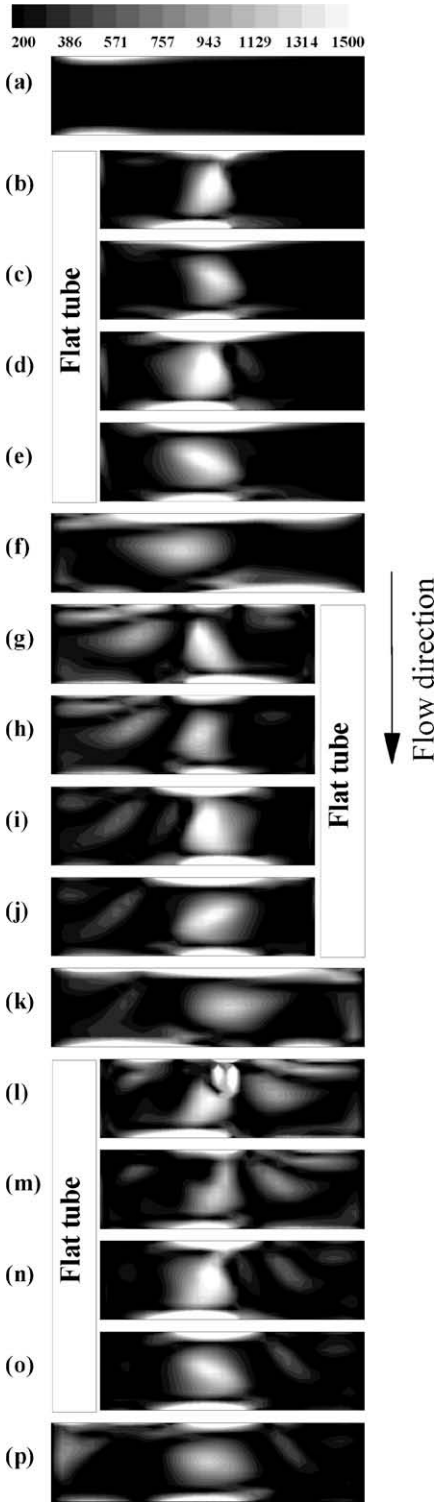

Fig. 9. Distribution of J^n_{ABS} on different cross-sections.

T_p is small, the same height of VGs, H/T_p increases; hence, the intensity of the secondary flow increases. Except at the leading edge of the fin, where Nu_s reaches its maximum and J^n_{ABS} has its very small value, Nu_s and J^n_{ABS} really have some significant relationship. As one expected, the secondary flow in most cases cannot change the boundary layer characteristics greatly, especially for internal flow in inlet region. Fig. 10 clearly states that in inlet region, the large Nu_s is not produced by the intensity of the second-

ary flow. Downstream the second VG located around the first tube row, the heat transfer enhancement produced by VGs is mainly caused by the secondary flow. Peak values of Nu_s appear in the locations of VGs. There has a similar distribution of compared with the distribution of Nu_s except at inlet region. The value of J^n_{ABS} reaches its peak values in front of the tube and in the locations of VGs.

There is no strong relationship between J^n_{ABS} and Nu_s in the inlet region, indicating clearly that J^n_{ABS} can account only for the contributions of the secondary flow to convective heat transfer. Other contributions to convection are not included in this parameter. In the inlet region, the intensity of convection is not determined by the secondary flow; hence, J^n_{ABS} cannot have the strong relationship with Nu_s.

5.3. Relationship between stream wise averaged J^n_{ABS} and the overall heat transfer intensity

The stream wise averaged absolute vorticity flux is defined as

$$J^n_{ABS,S} = \frac{1}{LA}\int\int\int_A |\omega^n| \, dAdx \tag{16}$$

The comparison of distribution of overall Nu, f and stream wise averaged $J^n_{ABS,s}$ as a function of Re for three fin spacing is shown in Fig. 11. It is found that the distribution of $J^n_{ABS,s}$ has the similar tendency as Nu. Both the Nu and the absolute vorticity flux increase with increasing of Re and T_p. The differences of Nu and $J^n_{ABS,s}$ between T_p = 4 mm and 5 mm is a little smaller than that between T_p = 5 mm and 6 mm. There is nearly the same value of Nu and $J^n_{ABS,s}$ when Re is 200 for three types of fin spacing studied in this paper.

The value of f decreases with the increasing of Re and T_p, The difference of f between three fin spacing decreases with increasing of Re. The difference of f between T_p = 4 mm and 5 mm is larger than that between T_p = 5 and 6 mm; this is contrary to the difference of Nu and $J^n_{ABS,s}$ The detailed effects of the fin spacing on heat transfer and friction factor are already presented in Ref. [8], and we should not repeat here.

The above results are obtained at a condition when the fin surfaces are at uniform wall temperature, which means the fin efficiency is 1. When no uniform temperature is considered, the reported characteristics still hold. But there are some differences: If fluid prosperities dependence on temperature is not considered, when the thermal boundary condition is changed, J^n_{ABS} does not change, but the intensity of convective heat transfer will be changed; for example, when the fin efficiency is considered. This means that the intensity of convective heat transfer depends not only on but also on the thermal boundary condition. The detailed information about this topic will be presented elsewhere.

6. Conclusions

As mentioned in the introduction section, in most cases, the secondary flow is used to enhance convective heat transfer. Except for twisted-tape inserts, a parameter that can specify the intensity of the secondary flow in general case is strongly called for. If such parameter is found, the relationship between this parameter and heat transfer intensity should be checked. In this paper, we have made efforts to find such parameter and check its relationship with the Nusselt number. From facts stated in above sections, the following conclusions can be made:

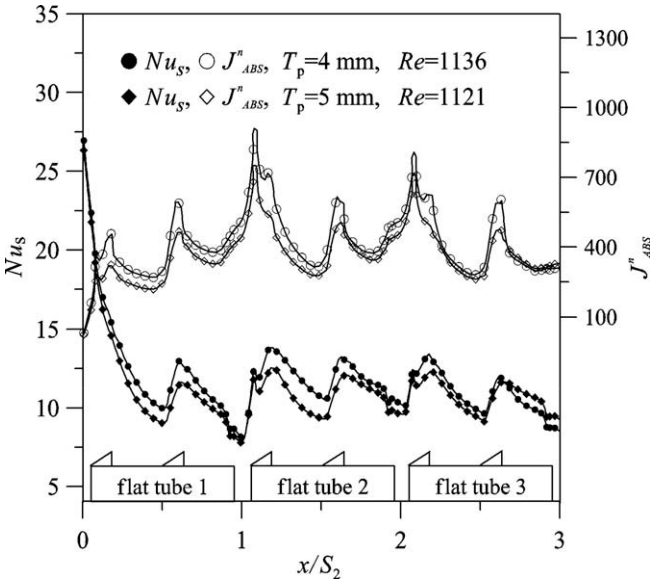

Fig. 10. Distribution of span-averaged Nu and J^n_{ABS} with fin spacing T_p = 4 and 5 mm.

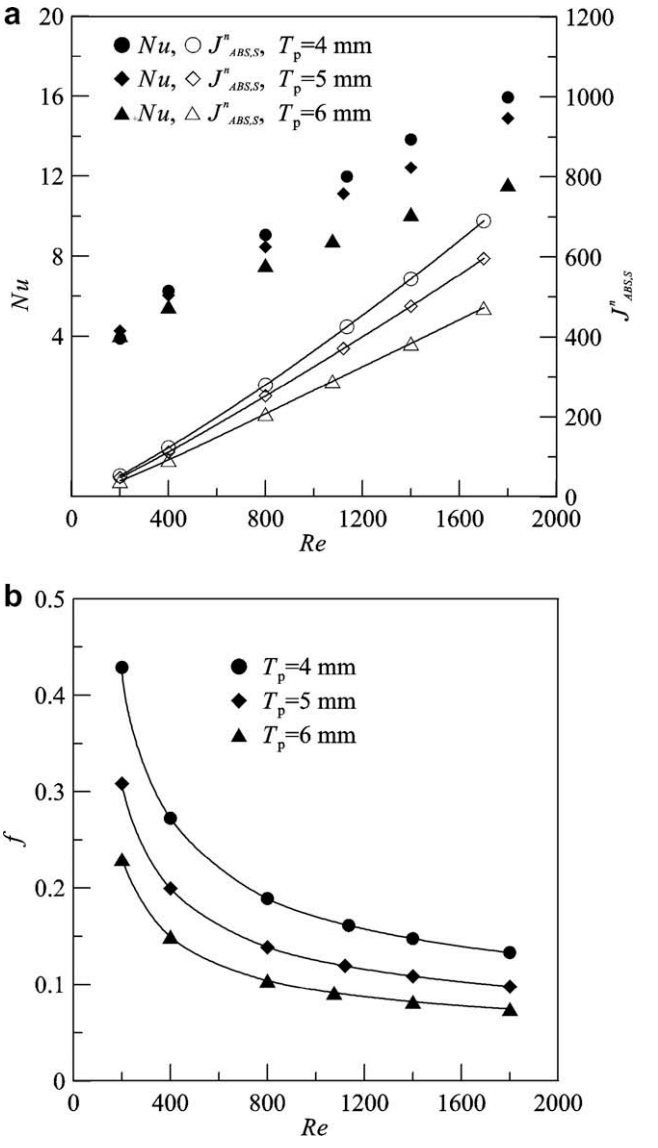

Fig. 11. Overall characteristics, (a) comparison of over all averaged Nu and stream wise averaged J^n_{ABS} at different Re and (b) friction factor.

1. The averaged absolute vorticity flux normal to the cross-section includes all vortices on this cross-section, and can be used to describe the intensity of the secondary flow.
2. Except at the beginning region of boundary layer, the span-averaged Nusselt number has nearly the same tendency with the cross-averaged absolute vorticity flux normal to the cross-section.
3. In most cases, the secondary flow cannot change greatly the boundary layer characteristics, especially for the internal flow at beginning region of boundary layer. The averaged absolute vorticity flux can account for only the secondary flow effects on convective heat transfer but cannot quantify the effects of developing boundary layer on convective heat transfer.
4. The stream wise averaged absolute vorticity flux normal to the cross-section has the same trend with the Nusselt number.

Acknowledgement

L.B. Wang acknowledges the support from the National Natural Science Foundation of China (No. 50876040).

References

[1] M. Fiebig, Vortex generators for compact heat exchangers, J. Enhanc. Heat Transfer 2 (1995) 43–61.
[2] M. Fiebig, Vortices, generators and heat transfer, Trans. IchemE A 76 (1998) 108–123.
[3] A. Valencia, M. Fiebig, N.K. Mitra, Heat transfer enhancement by longitudinal vortices in a fin-and-tube heat exchangers element with flat tubes, J. Heat Transfer 118 (1996) 209–211.
[4] M. Fiebig, A. Valencia, N.K. Mitra, Local heat transfer and flow losses in fin-tube heat exchanger with vortex generators: a comparison of round and flat tubes, Exp. Therm. Fluid Sci. 8 (1994) 35–45.
[5] A. Joardar, A.M. Jacob, Impact of leading edge delta-wing vortex generators on the thermal performance of a flat tube, louvered-fin compact heat exchanger, Int. J. Heat Mass Transfer 48 (2005) 1480–1493.
[6] L.B. Wang, F. Ke, S.D. Gao, Y.G. Mei, Local and average characteristics of heat/mass transfer over flat tube bank fin with four vortex generators per tube, J. Heat Transfer 124 (2002) 546–552.
[7] L.B. Wang, Y.H. Zhang, Y.X. Su, S.D. Gao, Local and average heat/mass transfer over flat tube bank fin mounted in-line vortex generators with small longitudinal spacing, J. Enhanc. Heat Transfer 9 (2002) 77–87.
[8] B.Z. Shi, L.B. Wang, F. Gen, Y.H. Zhang, The optimal fin spacing for three-row flat tube bank fin mounted with vortex generators, Heat Mass Transfer 43 (2006) 91–101.
[9] F. Ke, L.B. Wang, L. Hua, S.D. Gao, Y.X. Su, The optimum angle of attack of delta winglet vortex generators on heat transfer performance of finned flat tube bank with considering no uniform fin temperature, Exp. Heat Transfer 19 (2006) 227–249.
[10] Y.H. Zhang, L.B. Wang, Y.X. Su, S.D. Gao, Effects of span position of winglet vortex generator on local heat/mass transfer over a three-row flat tube bank fin, Heat Mass Transfer 40 (2004) 881–891.
[11] S.D. Gao, L.B. Wang, Y.H. Zhang, F. Ke, The optimum height of winglet vortex generators mounted on three-row flat tube bank fin, J. Heat Transfer 125 (2003) 1007–1016.
[12] S. Tiwari, D. Maurya, G. Biswas, V. Eswaran, Heat transfer enhancement in cross-flow heat exchangers using oval tubes and multiple delta winglets, Int. J. Heat Mass Transfer 46 (2003) 2841–2856.
[13] K. Torii, K.M. Kwak, K. Nishino, Heat transfer enhancement accompanying pressure-loss reduction with winglet-type vortex generators for fin-tube heat exchangers, Int. J. Heat Mass Transfer 45 (2002) 3795–3801.
[14] A. Jain, G. Biswas, D. Maurya, Winglet-type vortex generators with common-flow-up configuration for fin-tube heat, exchangers, Numer. Heat Transfer A 43 (2003) 201–219.
[15] A. Joardar, A.M. Jacobi, A numerical study of flow and heat transfer enhancement using an array of delta-winglet vortex generators in fin-and tube heat exchanger, J. Heat Transfer 129 (2007) 1156–1167.
[16] G. Biswas, K. Torii, D. Fujii, K. Nishino, Numerical and experimental determination of flow structure and heat transfer effects of longitudinal vortices in a channel flow, Int. J. Heat Mass Transfer 39 (1996) 3441–3451.
[17] Q.W. Wang, Q.Y. Chen, L. Wang, M. Zeng, Y.P. Huang, Z.J. Xiao, Experimental study of heat transfer enhancement in rectangular narrow channel with longitudinal vortex generators, Nucl. Eng. Des. 237 (2007) 686–693.
[18] L.H. Tang, M. Zeng, G.N. Xie, Q.W. Wang, Fin pattern effects on air-side heat transfer and friction characteristics of fin-and-tube heat exchangers with large number of large-diameter tube rows. Heat Transfer Eng. 30 (2009) 171–180.
[19] G.N. Xie, Q.W. Wang, B. Sunden, Parametric study and multiple correlations on air-side heat transfer and friction characteristics of fin-and-tube heat exchangers with large number of large-diameter tube rows, Appl. Therm. Eng. 29 (2009) 1–16.
[20] S. Liu, L.B. Wang, J.F. Fan, Y.H. Zhang, Y.X. Dong, K.W. Song, Tube transverse pitch effect on heat/mass transfer characteristics of flat tube bank fin mounted with vortex generators, J. Heat Transfer 130 (2008) 064501–064503.
[21] C.L. Zhu, L. Hua, D.L. Sun, L.B. Wang, Y.H. Zhang, Numerical study of interactions of vortices generated by vortex generators and their effects on heat transfer enhancement", Numer. Heat Transfer 50 (2006) 353–368.
[22] Z.Y. Guo, D.Y. Li, B.X. Wang, A novel concept of convective heat transfer enhancement, Int. J. Heat Mass Transfer 41 (1998) 2221–2225.
[23] R.L. Webb, Heat transfer and friction characteristics of internal helical-rib roughness, J. Heat Transfer 122 (2000) 134–142.
[24] P. Naphon, M. Nuchjapo, J. Kurujareon, Tube side heat transfer coefficient and friction factor characteristics of horizontal tubes with helical rib, Energy Convers. Manage. 47 (2006) 3031–3044.
[25] J.H. Kim, K.E. Jansen, M.K. Jensen, Analysis of heat transfer characteristics in internally finned tubes, Numer. Heat Transfer A 46 (2004) 1–21.
[26] R.M. Manglik, A.E. Bergles, Heat transfer and pressure drop correlations for twisted-tape inserts in isothermal tubes: Part I – laminar flows, J. Heat Transfer 115 (1993) 881–889.
[27] R.M. Manglik, A.E. Bergles, Heat transfer and pressure drop correlations for twisted-tape inserts in isothermal tubes: Part II – transition and turbulent flows, J. Heat Transfer 115 (1993) 890–896.
[28] G.C. Kidd Jr., Heat transfer and pressure drop for nitrogen flowing in tubes containing twisted tapes, AIChE J. 15 (1969) 581–585.
[29] O.H. Klepper, Heat transfer performance of short twisted tapes, AIChE J. 35 (1972) 1–24.
[30] S.K. Saha, U.N. Gaitonde, A.W. Date, Heat transfer and pressure drop characteristics of laminar flow in a circular tube fitted with regularly spaced twisted-tape elements, Exp. Therm. Fluid Sci. 2 (1989) 310–322.
[31] A.W. Date, U.N. Gaitonde, Development of correlations for predicting characteristics of laminar flow in a tube fitted with regularly spaced twisted-tape elements, Exp. Therm. Fluid Sci. 3 (1990) 373–382.
[32] L.M. Treffethen, R.B. Panton, Some unanswered questions in fluid mechanics, Appl. Mech. Rev. 110 (1990) 175–183.
[33] S.V. Patankar, Numerical Heat Transfer and Fluid flow, Hemisphere Publishing Co., New York, 1980. pp. 330–351.
[34] C.M. Rhie, W.L. Chow, Numerical study of the turbulent flow past an airfoil with trailing edge, separation, AIAA J. 21 (1983) 1525–1532.
[35] L.B. Wang, W.Q. Tao, Numerical analysis on heat transfer and fluid flow for arrays of non-uniform plate length aligned at angles to the flow direction, Int. J. Numer. Meth. Heat Fluid Flow 7 (1997) 479–496.
[36] P.R. Eiseman, A multi-surface method of coordinate generation, J. Comput. Phys. 47 (1979) 330–351.
[37] M. Fiebig, U. Brockmeier, N.K. Mitra, T. Guntermann, Structure of velocity and temperature fields in laminar channel flows with longitudinal vortex generators, Numer. Heat Transfer 15 (1989) 281–302.
[38] G. Biswas, P. Deb, S. Biswas, Generation of longitudinal stream-wise vortices – a device for improving heat exchanger design, J. Heat Transfer 116 (1994) 588–597.